

## Electrical conductivity of finite metallic systems: Disorder

Lucian Dulca, John Banhart, and Gerd Czycholl

*Institute for Theoretical Physics, University of Bremen, Kufsteiner Str. 2, 28359 Bremen, Germany*

(Received 10 November 1999)

The electrical conductivity of finite, three-dimensional clusters containing up to 201 atoms on an fcc lattice was calculated using a combination of density functional theory, multiple-scattering theory, and the Kubo-Greenwood equation. Isolated clusters and clusters embedded in a medium determined by the coherent-potential approximation (CPA) were investigated. Densities of states and electrical resistivities were calculated for various situations: varying numbers of configurations used for the configurational average, varying energies, different alloys, different cluster sizes, and, finally, two cluster types, namely, spherical and rectangular clusters. Cluster calculations were compared to CPA calculations based on the same alloys. From this comparison a criterion was derived when a representation of an infinite medium by finite clusters is expected to yield good results for the conductivity.

### I. INTRODUCTION

The electrical conductivity of multicomponent metallic systems is extremely sensitive to the microscopic arrangement of the various atom species on the crystal lattice. This is seen in alloys where ordered and disordered states exist. Such alloys, e.g.,  $\text{Cu}_3\text{Au}$ , show a comparatively high resistivity in the disordered phase,<sup>1,2</sup> whereas after the transition to the ordered state the resistivity drops to a very low value although during the transition merely some atoms are exchanged.<sup>2,3</sup>

The theoretical treatment of transport in disordered alloys has seen major advances since the advent of certain first-principle methods for the calculation of the electronic structure and the properties of such systems. In particular, an approach that starts from a *local density functional* description of the many-particle problem, treats disorder in the framework of the *coherent-potential approximation* (CPA) in conjunction with the *Korringa-Kohn-Rostoker* (KKR) method, and uses the rigorous *Kubo-Greenwood formula* of linear response theory for the transport calculation has led to excellent results for the conductivity of paramagnetic<sup>4-6</sup> and ferromagnetic alloys.<sup>7</sup> Even optical properties have been calculated making use of this formalism.<sup>8</sup>

Between perfectly ordered systems that in the limit of zero temperature do not show any electrical resistivity at all and random alloys, however, there is a wide range of systems that shows other states of order. One example is short-range order that is characterized by local correlations of the lattice occupation. Like long-range order short-range order has an influence on the electrical resistivity but the relative resistivity changes produced by this type of order are usually less than 5%.<sup>1,9</sup> In contrast to long-range order, which always leads to a reduction of electrical resistivity, short-range order can either increase or decrease resistivity. The theoretical treatment of short-range ordered systems is difficult because neither Bloch's theorem holds nor can an effective medium be introduced in a simple way as is done for random alloys. Short-range ordered systems have been treated in the framework of multiple-scattering theory by using small finite clusters. While expressions for "simple" electronic quantities

such as the density of states<sup>10</sup> have been obtained in a fairly easy way, the more complicated transport quantities have not been investigated very thoroughly up to now. To the knowledge of the authors short-range order effects on the electrical conductivity have only been studied by one group from first principles.<sup>5,11</sup> However, only two alloys were treated, and problems of configurational averaging and cluster size were not addressed.

This work aims on giving a thorough and systematic description of the electrical conductivity of finite clusters from first principles. In order to facilitate the calculations, only the case of disorder is treated. For this case cluster results can be compared to conductivities obtained by applying the coherent-potential approximation, which explicitly describes infinite disordered systems; however, omitting certain multi-site contributions. The three main objectives of the paper are (i) to clarify the influence of cluster size and the role of the procedure of configurational averaging, (ii) to compare cluster conductivities to corresponding CPA results, and (iii) to obtain predictions for which alloys or energy regimes cluster approximations are sufficiently precise to justify their application in short-range order calculations.

For this either large isolated clusters are constructed or clusters are embedded in a surrounding CPA medium representing the corresponding disordered alloy of the same composition. The electrical conductivity of these clusters is calculated using the Kubo-Greenwood formula in both cases. By considering different cluster configurations and by introducing statistical weights corresponding to the desired order parameter one hopes to be able to model disorder (or short-range order in a later stage). By calculating conductivities for three different alloys and for a variety of different energies one is able to explain the expected deviations of, e.g., cluster and CPA results, and to derive rules for which situation the cluster approximation works well.

The paper is organized as follows: In Sec. II the theoretical framework is outlined. Section III presents some first tests and the results of various sets of calculations. Section IV gives an interpretation of the results observed, which are finally summarized in Sec. V.

## II. THEORETICAL APPROACH

### A. Multiple-scattering theory

The application of multiple-scattering theory in electronic structure calculations has been discussed extensively in literature.<sup>12–15</sup> We therefore only give the most important equations relevant for the present work.

The potential function is assumed to be a collection of nonoverlapping muffin-tin potentials. The multiple-scattering theory leads to the following decomposition of the  $t$ -matrix for the system with respect to lattice sites:<sup>16</sup>

$$T(\vec{r}, \vec{r}'; \epsilon) = \sum_{nm} \tau^{nm}(\vec{r}, \vec{r}'; \epsilon). \quad (1)$$

The quantities  $\tau^{nm}$  are the scattering-path operators<sup>16</sup> and are defined by

$$\begin{aligned} \tau^{nm}(\vec{r}, \vec{r}'; \epsilon) &= t^n(\vec{r}, \vec{r}'; \epsilon) \delta_{nm} + \sum_{k \neq n} \int d^3 r_1 \int d^3 r_2 t^n(\vec{r}, \vec{r}_1; \epsilon) \\ &\times G_0^{nk}(\vec{r}_1, \vec{r}_2; \epsilon) \tau^{km}(\vec{r}_2, \vec{r}'; \epsilon), \end{aligned} \quad (2)$$

where  $t^n(\vec{r}, \vec{r}'; \epsilon)$  is the  $t$  matrix for a single potential well at site  $n$ .

We are interested in ‘‘on the energy shell’’ angular momentum components of the various scattering quantities describing elastic scattering. For the scattering-path operator they are given by

$$\begin{aligned} \tau_{LL'}^{nm}(\epsilon) &= \int d^3 r \int d^3 r' Y_L^*(\hat{r}) j_l(kr) \tau^{nm}(\vec{r}, \vec{r}'; \epsilon) j_{l'} \\ &\times (kr') Y_{L'}(\hat{r}'), \end{aligned} \quad (3)$$

where  $L \equiv (l, m)$ ,  $j_l$  are the spherical Bessel functions, and  $Y_L$  are complex spherical harmonics as given in Ref. 17.

The angular momentum expansion of the free-particle Green’s function is

$$\begin{aligned} G_0^{nm}(\vec{r}, \vec{r}'; \epsilon) &= \sum_{LL'} Y_L(\hat{r}_n) j_l(kr_n) \\ &\times G_{LL'}(\vec{R}_{nm}; \epsilon) j_{l'}(kr'_m) Y_{L'}^*(\hat{r}'_m), \end{aligned} \quad (4)$$

where  $\vec{r}$  is in the muffin-tin sphere around  $R_n$  and  $\vec{r}'$  in the muffin-tin sphere around  $R_m$  with  $n \neq m$  and  $\vec{r}_n = \vec{r} - \vec{R}_n$  and  $\vec{r}'_m = \vec{r}' - \vec{R}_m$ .  $G_{LL'}(\vec{R}_{nm}; \epsilon)$  in Eq. (4) are the real-space structure constants. They are given by<sup>18</sup>

$$\begin{aligned} G_{LL'}(\vec{R}_{nm}; \epsilon) &= -4\pi i k \sum_{L''} i^{l-l'-l''} C_{LL'L''}^{L''} h_{l''}^+(kR_{nm}) \\ &\times Y_{L''}^*(\hat{R}_{nm}), \end{aligned} \quad (5)$$

where  $h^+$  denote the outgoing Hankel functions and  $C_{LL'}^{L''}$  are the Gaunt coefficients defined by<sup>17</sup>

$$C_{LL'}^{L''} = \int d^3 k Y_L^*(\hat{k}) Y_{L'}(\hat{k}) Y_{L''}(\hat{k}). \quad (6)$$

Inserting Eq. (2) into Eq. (3) and taking Eq. (4) into account one obtains:

$$\begin{aligned} \tau_{LL'}^{nm}(\epsilon) &= t_L^n(\epsilon) \delta_{nm} \delta_{LL'} \\ &+ \sum_{k \neq n} \sum_{L''} t_L^n(\epsilon) G_{LL''}(\vec{R}_{nk}; \epsilon) \tau_{L''L'}^{km}(\epsilon). \end{aligned} \quad (7)$$

This is the fundamental multiple-scattering equation ‘‘on the energy shell.’’ It gives  $\tau_{LL'}^{nm}(\epsilon)$ , in terms of  $t_L^n(\epsilon)$ , which are completely determined by the phase shifts, and the structure constants  $G_{LL''}(\vec{R}_{nk}; \epsilon)$ , which depend only on the spatial arrangement of the scattering sites. Equation (7) is valid for any arrangement of potentials even if we have a different scatterer at each site. Thus, it is a good starting point to discuss pure metals as well as alloys with an arbitrary state of order.

A general expression for the Green’s function  $G(\vec{r}, \vec{r}'; \epsilon)$  for the assembly of scatterers that will be of use in later sections when we wish to obtain expressions for observables is<sup>19</sup>

$$\begin{aligned} G(\vec{r}, \vec{r}'; \epsilon) &= \frac{2m_e}{\hbar^2} \sum_{LL'} \{ Z_L^n(\vec{r}_n; \epsilon) \tau_{LL'}^{nm}(\epsilon) Z_{L'}^{*m}(\vec{r}'_m; \epsilon) \\ &- [Z_L^n(\vec{r}_n; \epsilon) J_L^{*n}(\vec{r}'_n; \epsilon) \theta(r'_n - r_n) \\ &+ J_L^n(\vec{r}_n; \epsilon) Z_L^{*n}(\vec{r}'_n; \epsilon) \theta(r_n - r'_n)] \delta_{LL'} \delta_{nm} \}. \end{aligned} \quad (8)$$

$Z_L^n(\vec{r}; \epsilon)$  is the regular solution of the radial wave equation while  $J_L^n(\vec{r}; \epsilon)$  is the corresponding irregular solution.  $\vec{r}, \vec{r}', \vec{r}_n$ , and  $\vec{r}'_m$  are the same as in Eq. (4).

Real systems contain a very large number of atoms. As the scattering equation (7) contains site indices one has to solve an equation containing extremely large matrices. As this is out of the reach of currently available computers one has to reduce the matrix dimensions occurring in the scattering equation. There are two possible ways for doing this: first, one can carry out a lattice Fourier transformation and transform the equation into  $k$  space, thus eliminating the site indices at all. This, however, is only possible if the system considered is translationally invariant. For pure metals or ordered alloys this is already given, but for disordered alloys this translational invariance has to be obtained by replacing the real system by an effective medium that represents the system as well as possible. One such medium is provided by the CPA. The second approach is to artificially cut out a region of the real system and to solve the multiple-scattering equations for this finite region, hoping that the effects one is discussing are spatially limited. Instead of looking at such isolated clusters one can also embed clusters in an infinite medium that is translationally invariant to avoid or minimize possible surface effects.

### B. Coherent-potential approximation

The CPA is one of the methods to obtain an effective medium that represents a real disordered alloy, or, more precisely, the configurational average of all possible arrangements of atoms that have the given macroscopic composi-

tion. The CPA condition for finding such an effective medium implies that a single impurity of any of the two (or more) atom species occurring in the alloy does not produce an extra scattering on the average. Because the condition refers to one lattice site the CPA is called a ‘‘single-site approximation.’’

In the language of multiple-scattering theory one describes the CPA by an ordered lattice of scatterers each represented by the same effective scattering amplitude  $t^{\text{CPA}}(\epsilon)$ . The problem is to find a suitable condition for this  $t$  matrix of the medium. In terms of the ‘‘on the energy shell’’ matrix elements of  $\tau^{nm}$  the CPA condition for an A-B alloy with concentrations  $c_A$  and  $c_B$  respectively, can be written as<sup>20</sup>

$$c_A \tau_A^{\text{CPA},00} + c_B \tau_B^{\text{CPA},00} = \tau^{\text{CPA},00}, \quad (9)$$

where the angular momentum indices have been omitted for matters of simplicity.  $\tau^{\text{CPA},00}$  describes the scattering of an ordered array of  $t^{\text{CPA}}$ 's situated at each of the lattice sites, whereas the  $\tau_\alpha^{\text{CPA},00}$  describe the same array except that at the central site there is an ‘‘impurity’’ of type  $\alpha \in \{A, B\}$ . Expressions for these impurity quantities have been derived.<sup>21,22</sup>

$$\tau_\alpha^{\text{CPA},00}(\epsilon) = \{1 + \tau^{\text{CPA},00}[(t^\alpha)^{-1} - (t^{\text{CPA}})^{-1}]\}^{-1} \tau^{\text{CPA},00}. \quad (10)$$

The lattice Fourier transform gives rise to an integral over the Brillouin zone of volume  $V_{BZ}$ :

$$\tau^{\text{CPA},00}(\epsilon) = \frac{1}{V_{BZ}} \int d^3k [(t^{\text{CPA}})^{-1} - G(\vec{k}; \epsilon)]^{-1}, \quad (11)$$

where  $G(\vec{k})$  are the  $k$ -space structure constants. The set of Eqs. (9), (10), and (11) are the fundamental equations for the effective scattering amplitude in the CPA, which is called KKR-CPA in this particular formulation because of its resemblance to the formulation of KKR band theory. They allow for a determination of  $(t^{\text{CPA}})^{-1}$  and  $\tau^{\text{CPA},00}$ , in general, by iteration. As one can calculate the density of states both as a function of energy and position from  $\tau^{\text{CPA},00}$ , one can carry out calculations determining the charge density self-consistently. Starting from some reasonable guess for the alloy potentials one solves the KKR-CPA equations, calculates a new potential, and continues until a final self-consistent potential has been obtained.

There is no limitation to the applicability of the theory arising from the size and energy dependence of the scattering amplitudes. In practical calculations one makes use of the fact that for most metals only the first few phase shifts matter so that only a small number of matrix elements of  $\tau$  and  $t$  have to be treated.

### C. Cluster methods

The second way to solve the multiple scattering equations (7) is to restrict the site indices to a small finite region. Then the equations can be solved in real space by simply inverting Eq. (7). One obtains

$$\tau_{LL'}^{nm} = [(t_L^n)^{-1} \delta_{nm} \delta_{LL'} - G_{LL'}^{nm}]_{LL'}^{-1}, \quad (12)$$

where  $t^n$  is the single-site  $t$ -matrix corresponding to the potential at site  $n$ .  $G^{nm}$  are the real-space structure constants given in Eq. (5). No reference to an external surrounding medium is taken *isolated cluster method* (ICM). In Eq. (12) we have to invert a matrix the dimension of which is  $(l_{max} + 1)^2 \times N$ , where  $N$  is the number of atoms in the cluster. For our purposes we chose  $l_{max} = 2$  and clusters up to 201 atoms, giving rise to matrices up to  $1809 \times 1809$  in size.

One can carry out self-consistent calculations with the cluster method by calculating charge densities from the results of Eq. (12) and by iterating the potential. In the present paper, however, the cluster equations were only solved for fixed potentials that were obtained from the KKR-CPA equations of the infinite medium.

The second cluster method is the *embedded cluster method* (ECM). A small finite cluster is embedded in a surrounding CPA medium that corresponds to the composition of the cluster. In this way one hopes to minimize surface effects by getting a smoother transition from the cluster into the surrounding space.

The expression for the scattering-path operator of an embedded cluster in a CPA medium is analogous to that of a single impurity [Eq. (10)] with the exception that simple matrices corresponding to the angular momentum representation have to be replaced by supermatrices also containing the cluster site indices. One obtains for  $\tau^{nm}$  (Ref. 15):

$$\tau_{LL'}^{nm} = (\{1 + \tau^{\text{CPA},nm}[(t^n)^{-1} - (t^{\text{CPA}})^{-1}]\delta_{nm}\}^{-1} \tau^{\text{CPA},nm})_{LL'}. \quad (13)$$

$\tau^{\text{CPA},nm}$  is the non-site-diagonal CPA scattering-path operator and is calculated by a generalization of Eq. (11):

$$\tau_{LL'}^{\text{CPA},nm}(\epsilon) = \frac{1}{V_{BZ}} \int d^3k \{[(t^{\text{CPA}})^{-1} - G(\mathbf{k}; \epsilon)]^{-1} \times e^{i\vec{k} \cdot (\vec{R}_n - \vec{R}_m)}\}_{LL'}. \quad (14)$$

As for isolated clusters the matrices occurring in Eq. (13) have the dimension  $(l_{max} + 1)^2 \times N$ . The embedded cluster method is a non-self-consistent approach because no account is taken of a possible change of the potentials by the existence of various clusters. However, one hopes that as long as the embedded clusters have about the same composition as the surrounding CPA medium, the deviations will not be so important.

### D. Calculation of density of states and conductivity

#### 1. Density of states

The density of states (DOS) of a CPA medium and at the central site of clusters is easily calculated using the respective form of the scattering-path operators [Eqs. (10), (12), or (13)] to calculate the Green function in Eq. (8). The DOS  $\rho$  at site  $n$  is then given by

$$\begin{aligned}
\rho(\epsilon) &= -\frac{1}{\pi} \int_{\text{cell } n} d^3r \text{Im } G(\vec{r}_n, \vec{r}_n, \epsilon) \\
&= -\frac{1}{\pi} \sum_{LL'} \int_{\text{cell } n} d^3r Z_L^n(\vec{r}, \epsilon) Z_{L'}^{*,n}(\vec{r}, \epsilon) \\
&\quad \times \begin{cases} \text{Im } \tau_{\alpha, LL'}^{\text{CPA}, nn}(\epsilon) & \text{CPA} \\ \text{Im } \tau_{LL'}^{nn}(\epsilon) & \text{cluster (isolated or embedded).} \end{cases}
\end{aligned} \tag{15}$$

## 2. Conductivity calculation

Linear-response theory provides very general expressions for transport coefficients which are exact in the limit of weak external fields. The diagonal components of the electrical conductivity tensor of a metallic conductor at zero temperature, i.e., with disorder originating from the atomic arrangement only, can then be written as

$$\sigma_{\mu\mu}(\epsilon) = \frac{\hbar}{\pi V} \langle \text{Tr}[J^\mu \text{Im } G(\epsilon) J^\mu \text{Im } G(\epsilon)] \rangle_{\text{conf}}. \tag{16}$$

Here  $V$  is the volume of the system, where  $J^\mu$  denotes the current operator in the  $\mu$ th spatial direction. The average has to be taken over all possible configurations of the system. The experimentally accessible conductivity is obtained by setting  $\epsilon = \epsilon_F$  in Eq. (16).

In terms of the scattering-path operator the Kubo-Greenwood equation can be rewritten as<sup>23</sup>

$$\begin{aligned}
\sigma_{\mu\mu}(\epsilon) &= -\frac{m_e^2}{\pi \hbar^3 V} \sum_{z_1, z_2} s_{z_1, z_2} \sum_{mn} \sum_{L_1, L_2, L_3, L_4} \\
&\quad \times \langle J_{L_4 L_1}^{\mu\mu}(z_1, z_2) \tau_{L_1 L_2}^{mn}(z_1) J_{L_2 L_3}^{n\mu}(z_1, z_2) \\
&\quad \times \tau_{L_3 L_4}^{nm}(z_2) \rangle_{\text{conf}},
\end{aligned} \tag{17}$$

where  $s_{z_1, z_2} = 2\delta_{z_1, z_2} - 1$ , and  $z_1$  and  $z_2$  are the complex energies  $z_{1,2} = \epsilon \pm i\eta$ , with  $\eta \rightarrow 0$ .  $\tau^{mn}$  are the cluster quantities defined in Eqs. (12) and (13) while the current operator is given by

$$J_{LL'}^{\mu\mu}(z, z') = -\frac{ie\hbar}{m} \int_{\text{cell } m} d^3r_m Z_L^m(\vec{r}_m, z) \frac{\partial}{\partial r_\mu} Z_{L'}^m(\vec{r}_m, z'). \tag{18}$$

For the case of a translationally invariant CPA medium the site index in Eq. (17) can be eliminated by a transformation to  $k$  space. Compact expressions for the conductivity can be obtained.<sup>23</sup>

## III. CALCULATIONS

### A. General parameters and definitions

For the calculation of the electronic structure of random alloys and finite clusters self-consistent alloy potentials were generated in a first step by iterating the KKR-CPA equations until charge self-consistency was achieved.<sup>24</sup> These potentials were used as a starting point for all further electronic structure calculations. Three situations were considered: the

TABLE I. Shells and clusters in a fcc lattice.

Shell	No. of sites in shell	Generating vector	Shell radius	No. of sites in cluster
0	1	(0.0, 0.0, 0.0)	0.0	1
1	12	(0.5, 0.5, 0.0)	0.5	13
2	6	(1.0, 0.0, 0.0)	1.0	19
3	24	(1.0, 0.5, 0.5)	1.5	43
4	12	(1.0, 1.0, 0.0)	2.0	55
5	24	(1.5, 0.5, 0.0)	2.5	79
6	8	(1.0, 1.0, 1.0)	3.0	87
7	48	(1.5, 1.0, 0.5)	3.5	135
8	6	(2.0, 0.0, 0.0)	4.0	141
9	24	(2.0, 0.5, 0.5)	4.5	165
10	12	(1.5, 1.5, 0.0)	4.5	177
11	24	(2.0, 1.0, 0.0)	5.0	201

infinite system described by the CPA, isolated clusters of a certain size where each lattice site was occupied by one of the alloy potentials, or clusters of a given size occupied by said potentials but embedded in a CPA medium. In all cases the density of states and the electrical conductivity were calculated. Clearly, only the single-site scattering case (CPA) is treated fully self-consistently in this way, whereas the treatment of the clusters was only approximately self-consistent. However, as in most calculations only clusters were permitted that had compositions corresponding to the macroscopic concentration, deviations from self-consistency should be small.

Angular momentum expansions were carried out up to a maximum value of  $l=2$  in all cases. A scalar relativistic approach including all relativistic effects except spin-orbit interaction was chosen. The Fermi energies determined in the KKR-CPA calculations were used for all the cluster calculations.

Two types of clusters were generated: spherical clusters, in which all lattice sites around a given central site up to a given cluster radius were included, and rectangular clusters containing all lattice sites within the space spanned by three orthogonal lattice vectors. Table I lists the size of spherical clusters and the number of sites in such clusters. Rectangular clusters were constructed as follows: we started from the 4 atoms in the fcc unit cell. In the first step we translated the atoms from the ( $y=0, z=0$ ) plane in the  $x$  direction by the lattice constant  $d$ . In the next step the atoms from the ( $y=d/2, z=d/2$ ) plane were translated in  $x$  direction too. The same procedure was then applied in the  $y$  and  $z$  directions. The number of translations need not be the same in each direction. Table II shows the dimensions of some rectangular clusters obtained with this construction.

The occupations of each lattice site of a given cluster were determined by using a random number generator. The occupation probability of each atom type was assumed to be proportional to the macroscopic concentration of the respective component. For most calculations an additional boundary condition was imposed on the construction of configurations: only configurations in which the number of  $A$  and  $B$  atoms corresponded to their macroscopic concentrations,  $c_A$  and  $c_B$ , respectively, were considered. For an  $A_{20}B_{80}$  alloy,

TABLE II. Rectangular clusters in a fcc lattice.

No. of $x$ translations	No. of $y$ translations	No. of $z$ translations	No. of sites
0	0	0	4
1	0	0	6
1	1	1	14
3	2	1	30
4	4	3	90
6	6	4	192

e.g., only configurations containing 20%  $A$  and 80%  $B$  atoms in the cluster were allowed. If necessary the occupation numbers were rounded to the next integer. Such configurations will be called “restricted” configurations.

Furthermore, in the configurational averages it was ensured that  $c_A N$  of a total of  $N$  configurations had an  $A$  atom at the central site, the remaining  $c_B N$  configurations having a  $B$  atom in the center. This condition is important only for the DOS calculation which is sensitive to the occupation of the central site.

Three different alloy systems were treated: the fcc alloy systems Ag-Pd and Cu-Pt and the fcc alloy  $\text{Mo}_{20}\text{Ni}_{80}$ . Ag-Pd is a “classical” alloy for discussing the electronic structure of disordered alloys. Already Mott used this alloy to demonstrate the influence of  $d$  bands on the transport properties of alloys<sup>25</sup> and many other authors did the same later. Cu-Pt is known to have a high residual resistivity that makes it attractive for cluster calculations as will be explained later.  $\text{Mo}_{20}\text{Ni}_{80}$  has an even higher resistivity and was used for cluster calculations by Nicholson and Brown.<sup>11</sup> Therefore, this alloy was also included in order to be able to compare results with those of Ref. 11 in a later stage of the work when short-range order is to be considered. Various sets of calculations were carried out: the number of configurations used for the average, the size of the involved clusters, the embedding medium (none or CPA) and the type of the clusters (spherical or rectangular) were varied.

### B. Symmetry tests

Prior to the actual calculations some tests were performed to check the correct implementation of the formalism. All possible configurations of a single-shell cluster (one central atom plus 12 neighboring atoms) in an fcc lattice, i.e.,  $2^{13} = 8192$  configurations, were divided into equivalence classes characterized by their equivalence under one of the 48 symmetry operations of the cubic symmetry group. There are 288 such equivalence classes.

The following tests were successfully carried out (i) the density of states and the trace of the conductivity tensor are identical for all members of one particular equivalence class; (ii) although various configurations belonging to the same equivalence class in general yield different diagonal elements of the conductivity tensor, the difference is always merely a permutation of the three spatial components; (iii) while for general occupations of the clusters with  $A$  or  $B$  atoms the three diagonal components of the conductivity tensor are different, degeneracies occur whenever the occupation shows certain symmetries. If, e.g., in a single shell clus-

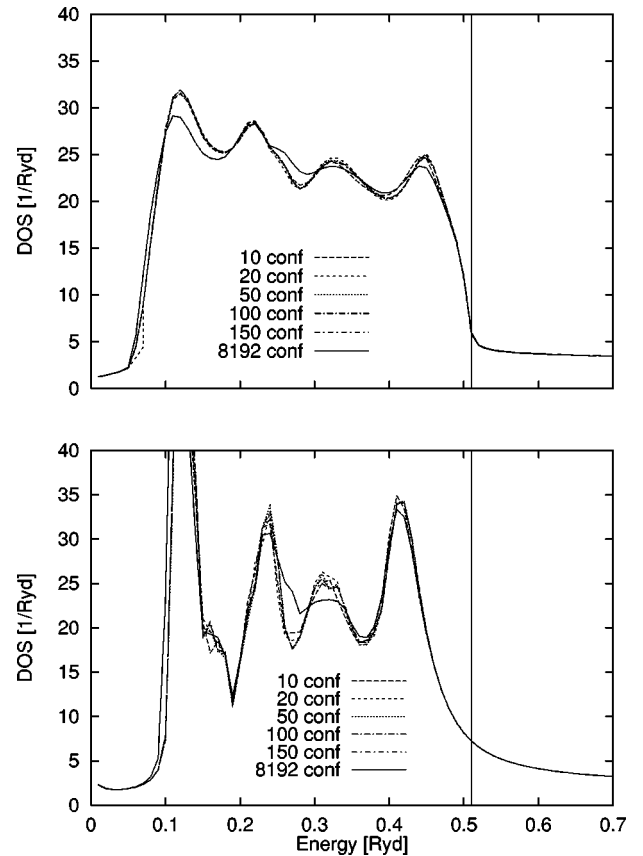


FIG. 1. Configurational averaged density of states of spherical single-shell (13 atoms) Ag-Pd clusters (embedded in a CPA medium, upper plot; isolated, lower plot) as a function of energy. Varying number of random configurations (restricted except for the case of 8192 configurations), cluster occupation in first shell:  $6 \times \text{Ag}$ ,  $6 \times \text{Pd}$ . Vertical line: Fermi energy.

ter the first shell contains only one  $A$  atom, the remaining atoms being of type  $B$ , two diagonal components of the conductivity tensor are identical.

### C. Calculations for entire bands

In a first set of calculations the density of states and the conductivity (and resistivity) were determined for energies covering the entire  $d$  band and some of the region above and below, i.e., between  $-0.1$  and  $0.7$  Ry above the muffin-tin zero for  $\text{Ag}_{50}\text{Pd}_{50}$ , between  $0.0$  and  $0.7$  Ry above the muffin-tin zero for  $\text{Cu}_{50}\text{Pt}_{50}$ , and between  $0.0$  and  $1.0$  Ry above the muffin-tin zero for  $\text{Mo}_{20}\text{Ni}_{80}$ . Calculations were carried out for each of a given set of restricted cluster configurations and for various cluster sizes. The single results were then averaged yielding configurationally averaged density of states and resistivities.

For single shell clusters (13 atoms) of silver and palladium atoms, various configurational averages including from 10 to 8192 (i.e., all, but of which only the 288 inequivalent configurations were treated explicitly) configurations were carried out in order to be able to assess the importance of the number of configurations necessary for a correct representation of disorder. Figure 1 shows the density of states at the central site of a single shell spherical cluster calculated by the embedded and isolated cluster method. Figure 2 shows the corresponding resistivities.

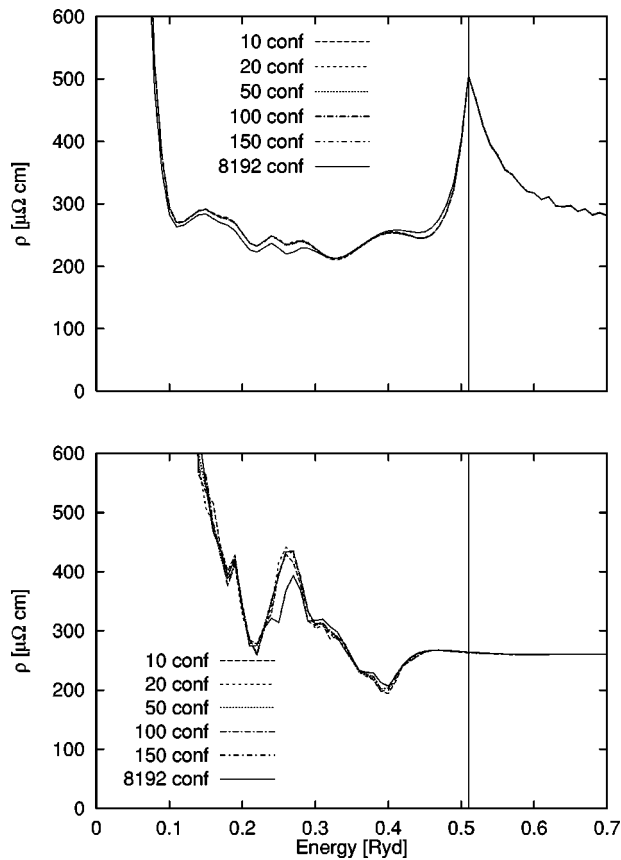


FIG. 2. Same as Fig. 1 for resistivity.

Another objective of the calculations was to investigate the behavior of the density of states and the resistivity as the number of shells is increased. Ten randomly chosen restricted configurations were used for the configurational average and spherical clusters containing up to seven shells (135 atoms) were constructed. Figure 3 shows the density of states at the central site of spherical Ag-Pd clusters for various cluster sizes calculated by the isolated and embedded cluster method. The clusters consist of equal numbers of Ag and Pd atoms. Figure 4 compares the resistivity of isolated and embedded clusters of various sizes. In all cases the results of CPA calculations are also shown for matters of comparison. Figures 5 and 6 give analogous data as shown in Fig. 4 for the alloys  $\text{Cu}_{50}\text{Pt}_{50}$  and  $\text{Mo}_{20}\text{Ni}_{80}$  ICM calculations only.

#### D. Calculations at the Fermi energy

A second set of calculations was carried out at the Fermi energy only. Spherical clusters containing up to 11 shells (201 atoms) were considered. The average was again performed over 10 restricted configurations (except for the zero-shell cluster, which only contains the central atom where only the two possible configurations were used). The three alloys  $\text{Ag}_{50}\text{Pd}_{50}$ ,  $\text{Cu}_{50}\text{Pt}_{50}$ , and  $\text{Mo}_{20}\text{Ni}_{80}$  were considered. Figures 7 and 8 show the density of states and the resistivity of clusters plotted as a function of cluster size (total number of shells and atoms given). The plots show the results for the single configurations as well as for the average. The corresponding CPA results are given by horizontal lines in Fig. 7, whereas the CPA resistivity has been subtracted from the

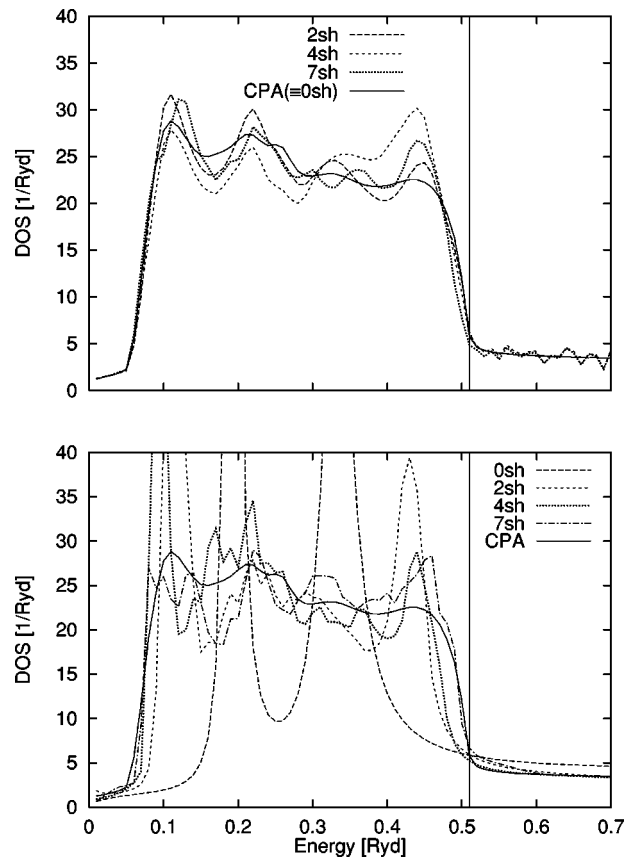


FIG. 3. Configurationally averaged density of states of spherical Ag-Pd clusters of various sizes (embedded in a CPA medium, upper plot; isolated, lower plot) as a function of energy (averaged with 10 restricted configurations, occupation of clusters: 50% Ag, 50% Pd). Vertical line marks Fermi energy.

cluster results in Fig. 8 to allow for displaying all results in one plot. In Fig. 7 the individual results for the density of states are marked differently according to the type of atom in the center of the cluster.

#### E. Calculations for varying alloy compositions

A third set of calculations was devoted to the comparison of different alloys. For this the whole range of Ag-Pd and

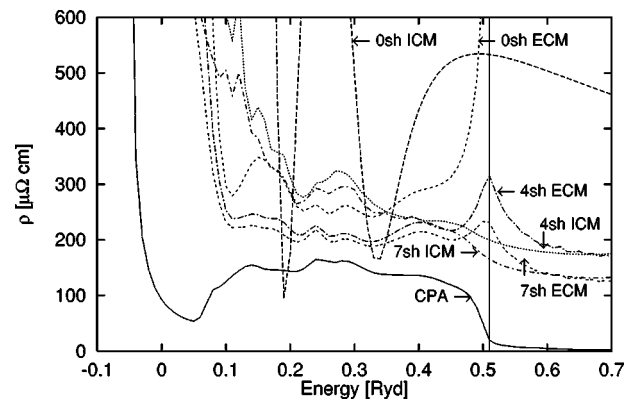


FIG. 4. Configurationally averaged resistivity of spherical Ag-Pd clusters of various sizes (embedded in a CPA medium, marked ECM; isolated clusters, marked ICM) as a function of energy (averaged with 10 restricted configurations, occupation of clusters: 50% Ag, 50% Pd). Vertical line marks the Fermi energy.

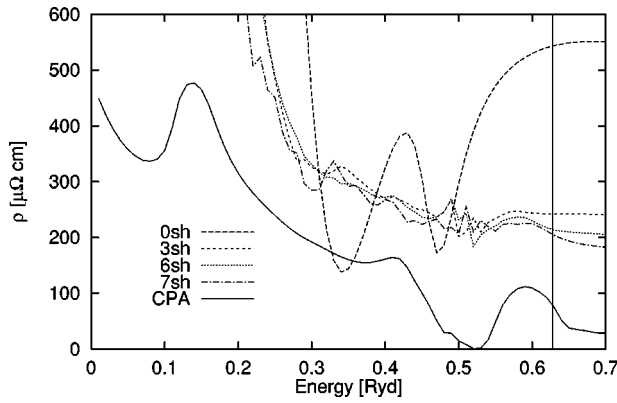


FIG. 5. Same as Fig. 4 for Cu-Pt (only isolated clusters). Occupation of clusters: 50% Cu, 50% Pt.

Cu-Pt alloys was considered. Figures 9 and 10 show resistivities at the Fermi energy averaged over 10 restricted random configurations of isolated clusters for each alloy as a function of concentration. Spherical clusters of various sizes up to 11 shells (201 atoms) were considered. CPA resistivities are given for matters of comparison.

#### IV. DISCUSSION

##### A. Configurational averaging

In order to assess the sensitivity of the configurationally averaged results to the number of configurations, various calculations were carried out with a single-shell cluster (13 atoms) based on various configuration numbers ranging from 10 to 8192. One can see from Fig. 1 that (i) the density of states shows a certain sensitivity to the number of configurations but only for energies close to the band edges, (ii) for most other energies quite precise results are already obtained for 10 configurations, (iii) the same is true for the resistivity shown in Fig. 2 and (iv) the full average is a bit different from the averages that merely contain restricted configurations due to the presence of the full range of configurations. These findings are important because they allow us to confine the calculations to a fairly low number of configurations thus saving much computation time.

##### B. Shell size dependence of density of states

The densities of states for the CPA and for embedded clusters do not deviate from each other very much (see Fig. 3

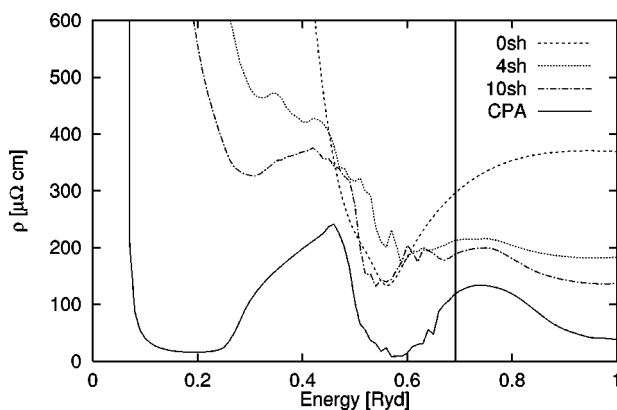


FIG. 6. Same as Fig. 4 for Mo-Ni (only isolated clusters). Occupation of clusters: 20% Mo, 80% Ni.

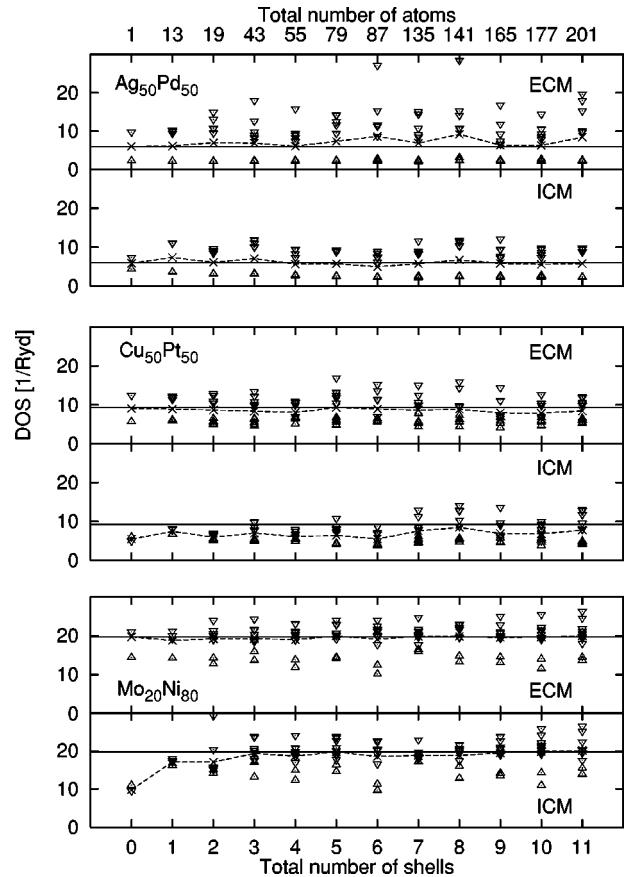


FIG. 7. Density of states of isolated (ICM) and embedded (ECM)  $\text{Ag}_{50}\text{Pd}_{50}$ ,  $\text{Cu}_{50}\text{Pt}_{50}$ , and  $\text{Mo}_{20}\text{Ni}_{80}$  clusters at the Fermi energy. Component projected DOS for single configurations ( $A$  atom in the center, up triangles;  $B$  atom in the center, down triangles, both DOS not concentration weighted) and the corresponding configurational averages of total DOS (crosses) are shown. CPA results are given by horizontal lines.

upper plot). This is easy to understand: for the zero-shell “cluster” this is exactly true, owing to the definition of the CPA as single-site average. For larger shells the cluster results deviate from the CPA values for two reasons: First, as only 10 configurations are taken into account in the configurational average, the sampling of disorder is not perfect, thus leading to some deviations (see Fig. 1). As will be shown later, the density of states is quite sensitive to the environment of a cluster. The restricted configurational average therefore might influence the density of states. Second, even if all configurations were included in an average (which is impractical for large cluster sizes) the DOS would deviate from the CPA because, on the one hand, the embedded cluster formalism is a non-self-consistent method, and on the other hand, the cluster method includes multisite effects that lead to a more complex electronic structure.

The density of states of isolated clusters (Fig. 3 lower plot) is quite different from that of embedded clusters. This is because especially for small clusters the neighborhood of the central site is quite different in an isolated cluster as compared to an embedded cluster. Figure 3 nicely shows how the bands are formed as the cluster size is increased. For the zero-shell “cluster” (only central atom) two pronounced peaks are present. They are the sum of the density of states

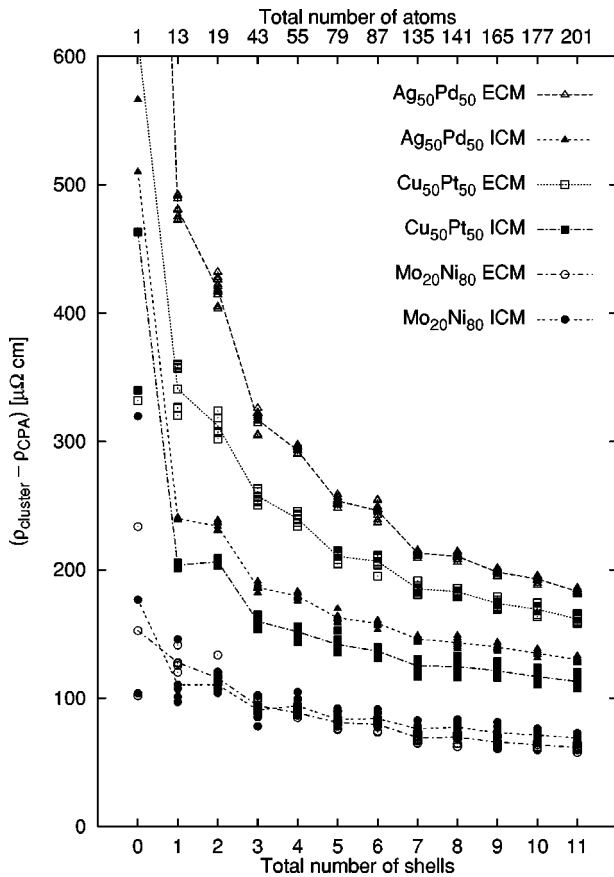


FIG. 8. Resistivities of isolated (ICM) and embedded (ECM) clusters at the Fermi energy for  $\text{Ag}_{50}\text{Pd}_{50}$ ,  $\text{Cu}_{50}\text{Pt}_{50}$ , and  $\text{Mo}_{20}\text{Ni}_{80}$ . Results for the ten restricted configurations and the corresponding configurational averages are shown. Resistivities are given relative to the CPA resistivity ( $\text{Ag}_{50}\text{Pd}_{50}$ ,  $23.1 \mu\Omega \text{ cm}$ ;  $\text{Cu}_{50}\text{Pt}_{50}$ ,  $80.2 \mu\Omega \text{ cm}$ ;  $\text{Mo}_{20}\text{Ni}_{80}$ ,  $120 \mu\Omega \text{ cm}$ ).

of a single silver and a single palladium atom. Both densities of states are broadened in energy because one is dealing with energies belonging to the continuous spectrum of the single atom potentials. The two peaks are centered at the energies where the two components have their  $d$  like scattering resonances. As the cluster size is increased the  $d$  bands build up

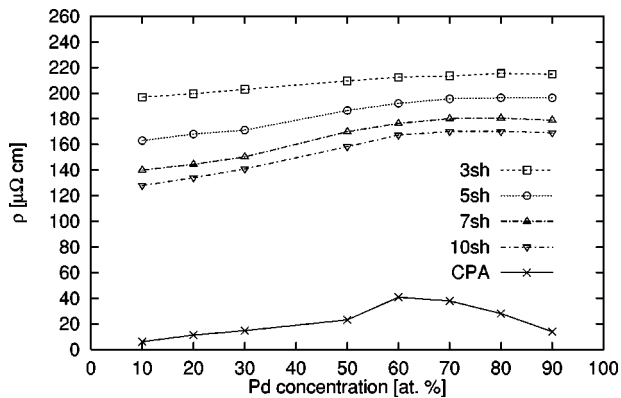


FIG. 9. Configurational averaged resistivity of Ag-Pd alloys calculated at the Fermi energy with finite isolated clusters (average over 10 restricted configurations, occupation with number of Ag and Pd atoms corresponding to macroscopic concentration). CPA results are given for matters of comparison.

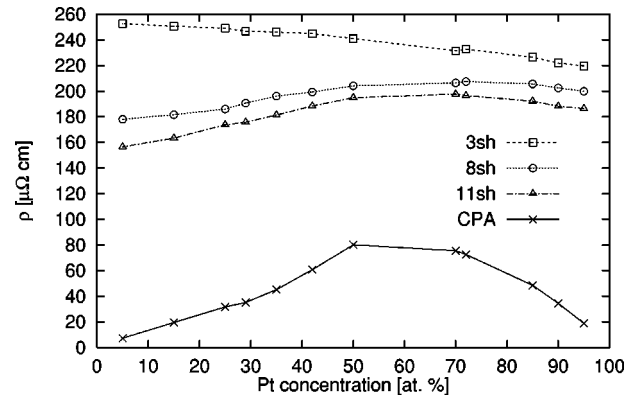


FIG. 10. Same as Fig. 9 for Cu-Pt.

and the cluster density of states moves closer and closer towards the corresponding rectangular shaped density of states of the CPA. However, one can still see some oscillations of the DOS especially near the band edges even for seven shells (135 atoms). This is typical for finite systems (see Refs. 20 and 26 for similar calculations). Only in the limit of very large (infinite) clusters is the density of states expected to get rounded off near the band edges and get close to the CPA result. However, even in this case multisite effects would lead to some residual differences.

### C. Shell size dependence of resistivity

Figures 4 to 6 show that the tendency observed for the density of states can also be found for the resistivity: Cluster resistivities get closer to the corresponding CPA resistivities as the shell number is increased. This is true for both types of clusters. Three energy regimes can be distinguished: (i) In the low energy regime the cluster resistivity, especially that of isolated clusters, takes very high values exceeding the CPA resistivity by a factor of 50 and more. This applies to all three alloys investigated. (ii) In an intermediate regime, which is almost the same as the regime of the  $d$  bands, the cluster resistivities get quite close to the CPA as the cluster size is increased. Embedded clusters (results only shown for Ag-Pd) lead to results slightly closer to the CPA than isolated clusters in this regime. (iii) Finally, for the energy regime above the  $d$  band complex, i.e., above the Fermi energy, the cluster resistivities deviate more from the CPA again. Especially Ag-Pd, where the CPA resistivity drops to very low values above the Fermi energy, shows this strong discrepancy. Moreover, for high energies embedded and isolated cluster resistivities converge towards the same value (see Fig. 4).

The explanation for the different regimes is straightforward: A cluster approach can only yield a correct resistivity if the mean free path of the conduction electrons is in the range of the cluster size or smaller. If the mean free path is much longer the scattering processes that are responsible for the finite resistivity cannot be expected to be included in the cluster representation anymore. As the resistivity takes its highest values for energies in the  $d$  bands of a transition metal (corresponding to short mean free paths) the cluster methods yield their best results in this energy regime. Using the CPA one clearly does not have this problem because the CPA treats an infinite averaged medium and is therefore ca-

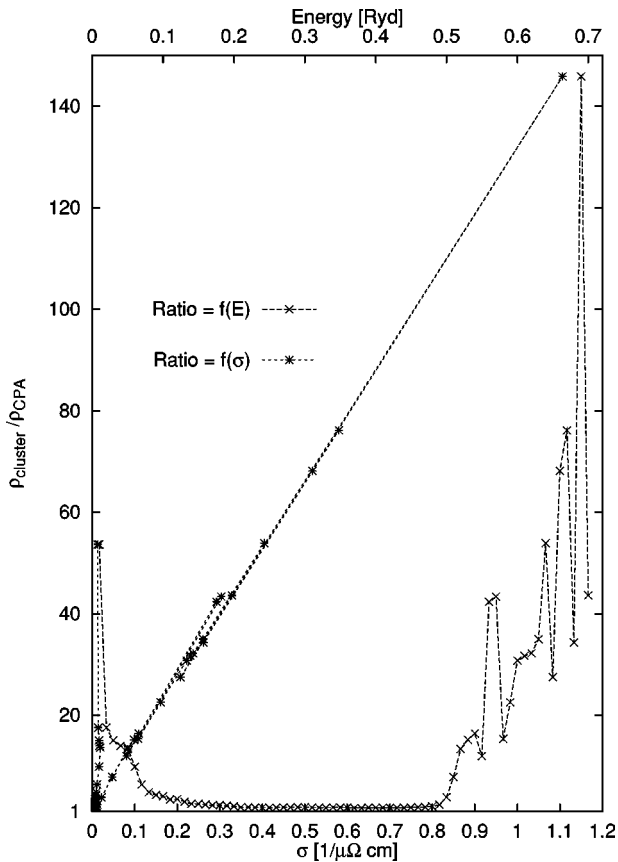


FIG. 11. Ratio of cluster and CPA resistivities ( $\rho_{\text{cluster}}/\rho_{\text{CPA}}$ ) for  $\text{Ag}_{50}\text{Pd}_{50}$  shown as a function of energy and CPA conductivity,  $f(E)$  and  $f(\sigma)$ , respectively. Calculations based on isolated seven-shell clusters and 10 restricted configurations.

pable of treating any mean free path. In contrast, approximations with small clusters only work well for systems with strong scattering (high resistivity). It is important to emphasize that the fact that cluster resistivities getting closer to the corresponding CPA values with increasing cluster sizes does not mean that there is an actual convergence. Convergence cannot be expected because even a very large (infinite) cluster would give results deviating from the CPA because cluster calculations include multisite effects that cannot be treated within a single-site formalism such as the CPA.

That the interpretation given is indeed plausible can be seen by looking at the deviation of cluster and CPA resistivities expressed by the ratio  $\rho_{\text{cluster}}/\rho_{\text{CPA}}$  as a function of both energy and CPA conductivity as it is displayed in Fig. 11. The ratio as a function of energy shows high values for low energies, i.e., below about 0.1 Ry, and energies above about 0.5 Ry as one can of course already see from Fig. 4. Looking at the ratio as a function of conductivity one finds an almost linear relationship except for the lowest energies. Therefore, the smaller the CPA conductivity is (indicating a short mean free path), the smaller the ratio between cluster and CPA resistivities. Extrapolating the conductivity to zero one sees that the ratio tends towards one. This means that the cluster resistivities get very close to the CPA if the mean free path is negligible compared to the cluster diameter. However, as already pointed out, one cannot expect an exact agreement because of the principal differences between single-site CPA and cluster expansions that contain multisite effects.

#### D. Density of states at the Fermi energy

The densities of states of various isolated and embedded clusters at the Fermi energy are shown in Fig. 7. It is evident that the values for individual configurations scatter greatly, even if the atom in the center (at which the DOS is calculated) is the same. The spread of the results is smaller for isolated clusters than for embedded clusters. Looking at the results more closely, one finds the following. (i) For the two alloys of an  $s$ -band metal (Ag, Cu) with a  $d$ -band metal (Pd, Pt), the DOS is low for the  $s$ -band atom at the center and high for the  $d$ -band metal at the center. (ii) The configurations with the  $s$ -band metal at the center are less sensitive to the occupation in the surrounding cluster than those with a  $d$ -band metal in the center. (iii) For the configurations with a  $d$ -band metal in the center very high DOS values (e.g., about 30 states/Ry for Ag-Pd) are found for configurations with many other  $d$ -band metal atoms in the cluster. These findings are not surprising if we note that for a pure  $d$ -band metal the Fermi energy lies in a region where the density of states is high and has a rich structure as a function of energy. Changes in the environment of a  $d$ -band atom therefore cause a strong change of the DOS, whereas the DOS of an  $s$ -band metal—in which the Fermi energy lies in the flat  $s$  band with a low DOS—is relatively insensitive to the composition of its neighborhood.  $\text{Mo}_{20}\text{Ni}_{80}$  with two  $d$ -band constituents consequently shows about the same behavior of the DOS no matter which of the atoms is in the center.

The averages of 10 restricted configurations (only two for zero-shell “clusters”) can be compared with the CPA density of states. One finds that (i) for a zero-shell embedded “cluster” the two quantities are the same by definition of the CPA; (ii) the averaged embedded cluster DOS is quite close to the CPA DOS for all cluster sizes (see discussion in Sec. IV B); and (iii) the averaged isolated cluster densities of states deviate more from the CPA DOS especially for small clusters. The isolated zero-shell “cluster” DOS is far away from the CPA result in  $\text{Mo}_{20}\text{Ni}_{80}$ , in which the Fermi energy is close to the band edge where such deviations tend to be more pronounced (see Sec. III D and Fig. 3) and quite close to the CPA DOS for  $\text{Ag}_{50}\text{Pd}_{50}$ , in which the Fermi energy is far above the band edge. For large isolated clusters all densities of states move towards the CPA as expected.

#### E. Resistivity at the Fermi energy

Turning to the resistivity, which is shown in Fig. 8 for ten restricted configurations and as a configurational average for both isolated and embedded clusters of varying sizes, one notes the following. (i) In contrast to the density of states the resistivity is strongly cluster size dependent. (ii) The scatter between individual configurations is much smaller than for the DOS. (iii) An increase of cluster size leads to averaged resistivities that slowly approach the CPA resistivity (which is represented by the value 0 in Fig. 8). (iv) The resistivities lie closest to the CPA for  $\text{Mo}_{20}\text{Ni}_{80}$ , followed by  $\text{Cu}_{50}\text{Pt}_{50}$  and  $\text{Ag}_{50}\text{Pd}_{50}$ . (v) Isolated and embedded clusters show a similar tendency. For  $\text{Ag}_{50}\text{Pd}_{50}$  and  $\text{Cu}_{50}\text{Pt}_{50}$  isolated clusters lead to lower resistivities while for  $\text{Mo}_{20}\text{Ni}_{80}$  the opposite is true. (vi) The changes in resistivity when one increases the cluster size are more pronounced for small clusters and when the shell added has many atoms.

The behavior of the density of states differs from that of the resistivity because the DOS is a local quantity describing the electronic structure at one particular location in the cluster (the center), whereas for the resistivity all sites of a cluster are treated in the same way. Moreover, from what was said in Sec. IV C one knows that the resistivity is strongly shell-size dependent especially when the mean free path is in the range or larger than the shell diameter because then the scattering process cannot be represented properly and each increase in shell size adds significant contributions to the resistivity. Only when the mean free path is much shorter than the diameter of the cluster would one expect that the resistivity saturated as a function of shell size. Such an effect does not clearly exist for the density of states, which is not influenced very much by distant atoms. For  $\text{Cu}_{50}\text{Pt}_{50}$  a mean free path of 1.7 nm was determined from the Boltzmann equation as described in Ref. 27, which corresponds to about 4.5 lattice spacings or slightly less than the diameter of a five-shell cluster. For  $\text{Ag}_{50}\text{Pd}_{50}$  the mean free path is about three times as long, for  $\text{Mo}_{20}\text{Ni}_{80}$  it is about half the mean free path for  $\text{Cu}_{50}\text{Pt}_{50}$ . This explains well the magnitude of deviation between cluster resistivities and CPA as seen in Fig. 8, which increases from  $\text{Mo}_{20}\text{Ni}_{80}$  to  $\text{Cu}_{50}\text{Pt}_{50}$  and  $\text{Ag}_{50}\text{Pd}_{50}$ . From Fig. 8 it is also obvious that a convergence of the resistivity (to some “infinite cluster” value, not to the CPA resistivity) has not been achieved for 11-shell clusters (201 atoms) and that still larger clusters are necessary to obtain convergence.

#### F. Resistivity for different alloys

From what was discussed in the previous sections the results for the cluster resistivities for alloys of different compositions shown in Figs. 9 and 10 are not surprising. While the CPA calculation for the alloys Ag-Pd and Cu-Pt reveals the typical distorted Nordheim-like curve with a maximum near 60 and 50 at. % Pd or Pt, respectively, and the drop to zero resistivity for the pure components, the cluster resistivities do not show this behavior. The cluster results are closest to the CPA resistivity for binary alloys in about the middle of the composition range, while the deviations are largest for dilute alloys. Extrapolation of cluster results to pure components leads to finite resistivities while the (infinite) pure metal should have zero resistivity. This comparison can be visualized best by looking at the ratio between cluster resistivity and the corresponding CPA resistivity and plotting it as a function of composition (Fig. 12).

The reason for the better agreement of cluster resistivities with the corresponding CPA results for concentrated alloys clearly again lies in the shorter mean free path in these alloys as was already discussed before. To make this clear the mean free path is shown in Fig. 12 and compared to the deviation ratio. The former was determined by using the semiclassical Boltzmann equation.<sup>27</sup> The mean free path given is an average over all electrons in the innermost sheet of the Fermi surface. These electrons carry at least 80% of the electric current. The remaining sheets of the Fermi surface contain slow electrons with a much shorter mean free path. Figure 12 shows that mean free path and deviation ratio  $\rho_{\text{cluster}}/\rho_{\text{CPA}}$  are nearly proportional. Therefore, the larger the mean free path, the more one needs a large cluster in order to get a

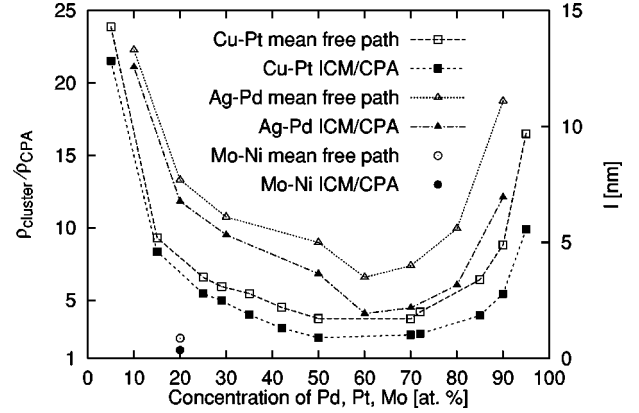


FIG. 12. Deviation of cluster from CPA resistivities expressed as the ratio  $\rho_{\text{cluster}}/\rho_{\text{CPA}}$  as a function composition ( $E=E_F$ ). Isolated 11-shell clusters and an average with 10 restricted configurations were used. Moreover, the mean free path of the electrons of the innermost sheet of the Fermi surface is given for each alloy.

realistic value for the cluster resistivity. For  $\text{Mo}_{20}\text{Ni}_{80}$ , e.g., the diameter of the 11-shell cluster used is equal to four times the mean free path (0.87 nm). This situation allows for a quite reasonable description of the resistivity by a cluster approximation, although the CPA resistivity is still lower by a factor of 1.7. For alloys such as  $\text{Ag}_{90}\text{Pd}_{10}$ , however, the mean free path is three times the diameter of the largest cluster used and the resistivity based on such clusters is completely wrong.

#### G. Influence of cluster type

So far only spherical clusters have been considered. It is important to raise the question of how important the particular cluster shape is. To give an answer two calculations were carried out with spherical and rectangular clusters of a similar size, namely a spherical cluster of six shells (87 atoms) and a rectangular cluster of 90 atoms. The alloy  $\text{Ag}_{50}\text{Pd}_{50}$  was chosen and 10 restricted configurations were used for the average in both cases. The results shown in Fig. 13 show that there is little difference between the two cluster types.

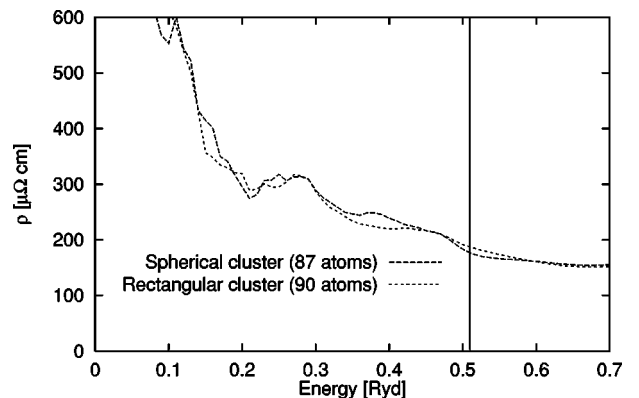


FIG. 13. Resistivity of isolated spherical clusters with six shells (87 atoms) compared to the resistivity of isolated rectangular clusters with 90 atoms. Cluster composition  $\text{Ag}_{50}\text{Pd}_{50}$ . 10 restricted configurations used for averaging.

### H. Comparison to experimental resistivities

Because comparing calculated results with measured data is not one of the main purposes of this paper, only a short look is given on such data. For the three alloys  $\text{Ag}_{50}\text{Pd}_{50}$ ,  $\text{Cu}_{50}\text{Pt}_{50}$ , and  $\text{Mo}_{20}\text{Ni}_{80}$  the experimental resistivity extrapolated to  $T=0$  is 29 (Ref. 28), 82 (Ref. 3), and 117 (Ref. 29) (all in  $\mu\Omega$  cm), respectively. Our CPA calculations yield 23.1, 80.2, and 120, respectively. Reference 11 gives  $116 \mu\Omega$  cm for the latter case. The observed excellent agreement between experimental and calculated resistivities, however, is partially lost when one includes angular momenta up to  $l=3$  in the calculations. The resistivity of  $\text{Mo}_{20}\text{Ni}_{80}$ , e.g., drops to  $71 \mu\Omega$  cm, and a similar drop is observed for other alloys.<sup>6</sup> Calculated CPA resistivities are lower than corresponding experimental values for many alloy systems—provided that sufficiently high angular momenta are taken account of—indicating that there are scattering mechanisms in real alloys that cannot be included in the CPA. The cluster approximations treated in this paper could perhaps yield better results, although nothing definite can be said until a convergence with respect to the cluster size has been achieved.

### V. CONCLUSIONS AND OUTLOOK

By calculating the density of states and the electrical conductivity (or resistivity) of finite clusters that were either isolated or embedded in a surrounding CPA medium, the possibility for approximately representing an infinite lattice by finite clusters could be evaluated. In the work presented here it was attempted to approximate a disordered system described by the CPA by finite clusters and an explicit configurational average over various cluster configurations.

It was found that especially for the conductivity a small number of configurations is sufficient for the average because the conductivity is quite insensitive to the arrangement of the atoms in a cluster. Resistivities of clusters were calculated and compared with corresponding results given by the CPA for various situations: energy dependent resistivities were calculated, quantities only at the Fermi level were given a closer look and, finally, various alloys were treated for matters of comparison. The general result obtained was that (i) the larger the clusters, the closer the results lie to the CPA, and (ii) cluster and CPA resistivities are quite close together whenever the resistivity of the system is high, or, the mean free path of conduction electrons is small compared to the cluster diameter. In the alloys considered this is true for energies that lie in the  $d$ -band complex. Therefore, the cluster methods yield good results for the resistivity only if the Fermi level lies in the  $d$  band. Not very much difference was seen between the conductivity of isolated and embedded clusters so that most calculations were performed within the simpler isolated cluster scheme.

It seems realistic that for highly resistive alloys short-range order effects can be modeled by including statistical weights in the configurational average. There is some hope that the resistivity change associated with a rearrangement of atoms after short-range ordering can be calculated this way. In a forthcoming paper<sup>30</sup> the cluster methods presented in this paper will therefore be applied to some highly resistive alloys in various states of order.

### ACKNOWLEDGMENT

The work presented was funded by the Deutsche Forschungsgemeinschaft (project Cz 31/10-1).

- 
- <sup>1</sup>P.L. Rossiter, *The Electrical Resistivity of Metals and Alloys* (Cambridge University Press, Cambridge, UK, 1987).
- <sup>2</sup>K. Schröder, *CRC Handbook of Electrical Resistivities* (CRC Press, Boca Raton, FL, 1983).
- <sup>3</sup>C.H. Johansson and J.O. Linde, *Ann. Phys. (Leipzig)* **82**, 449 (1927).
- <sup>4</sup>J.C. Swihart, W.H. Butler, G.M. Stocks, D.M. Nicholson, and R.C. Ward, *Phys. Rev. Lett.* **57**, 1181 (1986).
- <sup>5</sup>R.H. Brown, P.B. Allen, D.M. Nicholson, and W.H. Butler, *Phys. Rev. Lett.* **62**, 661 (1989).
- <sup>6</sup>J. Banhart, *Philos. Mag. B* **77**, 106 (1998).
- <sup>7</sup>J. Banhart and H. Ebert, *Europhys. Lett.* **32**, 517 (1995).
- <sup>8</sup>J. Banhart, *Phys. Rev. Lett.* **82**, 2139 (1999).
- <sup>9</sup>W. Pfeiler, *Acta Metall.* **36**, 2417 (1988).
- <sup>10</sup>J. Banhart, P. Weinberger, and J. Voitländer, *Phys. Rev. B* **40**, 12 079 (1989).
- <sup>11</sup>D.M.C. Nicholson and R.H. Brown, *Phys. Rev. Lett.* **21**, 3311 (1993).
- <sup>12</sup>H. Ehrenreich and L. Schwartz, in *Solid State Physics*, edited by H. Ehrenreich, F. Seitz, and D. Turnbull (Academic Press, New York, 1976), Vol. 31, p. 149.
- <sup>13</sup>J.S. Faulkner, in *Progress in Material Science*, edited by J.W. Christian, P. Haasen, and T.B. Massalski (Pergamon Press, New York, 1982), Vol. 27, p. 1.
- <sup>14</sup>P. Weinberger, *Electron Scattering Theory for Ordered and Disordered Matter* (Clarendon Press, Oxford, 1990).
- <sup>15</sup>A. Gonis, *Green Functions for Ordered and Disordered Systems* (Elsevier, North-Holland, 1992).
- <sup>16</sup>B.L. Györffy and M.J. Stott, in *Band Structure Spectroscopy of Metals and Alloys*, edited by D.J. Fabian and L.M. Watson (Academic Press, London, 1973), p. 385.
- <sup>17</sup>C. Cohen-Tannoudji, B. Diu, and F. Lalöe, *Quantum Mechanics* (Herrman, Paris, 1977).
- <sup>18</sup>J.S. Faulkner, *J. Phys. C* **10**, 4661 (1977).
- <sup>19</sup>J.S. Faulkner and G.M. Stocks, *Phys. Rev. B* **21**, 3222 (1980).
- <sup>20</sup>H. Winter and G.M. Stocks, in *The Electronic Structure of Complex Systems*, Vol. 113 of *NATO Advanced Studies Institute, Series B: Physics*, edited by P. Phasiseau and W.M. Temmermann (Plenum Press, New York, 1983), p. 463.
- <sup>21</sup>P. Soven, *Phys. Rev. B* **2**, 4715 (1970).
- <sup>22</sup>B.L. Györffy, *Phys. Rev. B* **5**, 2382 (1972).
- <sup>23</sup>W.H. Butler, *Phys. Rev. B* **31**, 3260 (1985).
- <sup>24</sup>CPA computer program by H. Akai used.
- <sup>25</sup>N.F. Mott and H. Jones, *The Theory of the Properties of Metals and Alloys* (Dover, New York, 1958).
- <sup>26</sup>H. Winter and G.M. Stocks, *Phys. Rev. B* **27**, 882 (1983).
- <sup>27</sup>J. Banhart, P. Weinberger, and J. Voitländer, *J. Phys.: Condens.*

- Matter **1**, 7013 (1989).
- <sup>28</sup>B.R. Coles and J.C. Taylor, Proc. R. Soc. London **267**, 139 (1962).
- <sup>29</sup>T.S. Lei, K. Vasudevan, and E.E. Standbury, in *High-Temperature Ordered Intermetallic Alloys*, edited by C. C. Koch *et al.*, MRS Symposia Proceedings No. 39 (Materials Research Society, Pittsburgh, 1985), p. 163.
- <sup>30</sup>L. Dulca, J. Banhart, and G. Czycholl (unpublished).